Arugonda Rakesh
Vakamalla T. S. R
Kumar Reddy
Mangadoddy Narasimha

Indian Institute of Technology Hyderabad, Department of Chemical Engineering, Ordinance Factory Estate, Yeddumailaram, India.

Air-Core Size Measurement of Operating Hydrocyclone by Electrical Resistance Tomography

Electrical resistance tomography (ERT) allows to measure hydrocyclone internal flow dynamics in situ. A dual-plane high-speed ERT system is proposed to map two-phase distributions with varying operational parameters. Experimental results are presented in terms of air-core diameter and its size variation for various feed flow rates and design variables. The total variation algorithm provides the best results compared to Tikhonov and Gauss-Newton algorithms. The influence of finite element method mesh size on air-core resolution is evaluated. High-speed video imaging and a volume-of-fluid-based two-phase computational fluid dynamics (CFD) model are adopted to determine the air-core size. Cross validation of air-core size and shape is performed by ERT measurements with CFD simulations and high-speed video imaging.

Keywords: Air-core, Electrical resistance tomography, Hydrocyclone, Two-phase CFD

Received: September 30, 2013; *revised:* February 26, 2014; *accepted:* February 27, 2014

DOI: 10.1002/ceat.201300672

1 Introduction

Hydrocyclones are widely used as separators or classifiers in chemical, environmental, and mineral processing industries to separate solid particles from a solid-liquid suspension based on the size of particles. A hydrocyclone works on the principle of centrifugal sedimentation in which particles are separated from the liquid by centrifugal force. The slurry is tangentially injected into the hydrocyclone to develop a centrifugal force. This force generates vortex motion to the fluid inside the hydrocyclone. The outer vortex, which is formed near to the wall of the hydrocyclone, flows downward and carries coarse particles to the underflow. The inner vortex, which is formed along the central axis, flows upward with the clean fluid or the fluid with fine particles. Due to the formation of vortex, a low-pressure region prevails along the axis. This low-pressure region is filled by air through the underflow and the overflow orifices from the atmosphere. Thus, the air-core is formed along the axis of the hydrocyclone.

The air-core is one of the most important flow characteristics in hydrocyclones. The stability of the cyclone is dictated by air-core formation. Careful control of the air-core is necessary for efficient operation. Air-core information is of high importance for design and selection of a hydrocyclone. Numerous techniques are described in the literature for the measurement of air-core in industrial cyclones, such as gamma ray tomography (GRT), electrical resistance tomography (ERT), electrical impedance tomography (EIT), high-speed video imaging etc.

ERT is one such technique to measure the air-core and flow visualization in situ. As the air phase has low conductivity compared to water, air-core formation in the hydrocyclone can be easily visualized by adopting the ERT system. It offers complementary and relatively low-cost measurements in multiphase flow applications such as solid/liquid in hydrocyclone flow visualization, high-speed flow imaging in slurry conveying systems, and spatial concentration of the dispersed phases in pipelines, separators, and reactors [1–6]. ERT employs conductive sensors on the wall of the process vessel to inject current and then sense voltage differences from which the conductivity of the electrolyte inside the process vessel can be measured by forward and inverse approaches.

Analysis of the raw data enables conversion into images by means of a reconstruction algorithm. The reconstruction processes have their own limitations and require careful application to avoid misinterpretation. The reconstruction of the images is independent of the parameters of a specific process; it is based entirely on the results obtained from the measurement and the image reconstruction algorithm. The choice of image reconstruction algorithm is a trade-off between accuracy of image and time required for reconstruction. Mapping of the distribution of concentration enables calculation of the parameters of the fluid such as the concentration profiles. In particular, the most employed reconstruction techniques in ERT are filtered back projection between equipotential lines [7], back projection using a sensitivity coefficient [8], perturbation method [9], double-constraint method [10], Newton-Raphson method [11], and the sensitivity conjugate gradient (SCG) method [12].

Correspondence: Dr. Mangadoddy Narasimha (narasimha@iith.ac.in), Indian Institute of Technology Hyderabad, Department of Chemical Engineering, Ordinance Factory Estate, Yeddumailaram, 502205, India.

2 Literature

The classical literature on hydrocyclones relates only rarely to the air-core measurement, although in the 1990s some investigations were performed by a number of researchers [13–16]. In particular, the mechanisms of separation and models of fluid flow in hydrocyclone separators have been studied but are still not completely understood. Because of their complex nature due to high swirl and varying turbulence conditions, the presence of an air-core interface inside the separator, and control of the separator, one has to rely on the empirical approaches in the past [17–19]. Non-intrusive measurements such as ERT and computational fluid dynamics (CFD) are effective techniques to understand the internal flow of the hydrocyclone separator. A number of researchers attempted to characterize the hydrocyclone flow by ERT/EIT in the past [4, 5, 20–24]. Williams et al. [25] and Gutiérrez et al. [26] described the controlling of underflow discharge using ERT. They also measured the air-core diameter and concentration profiles for different operational parameters of hydrocyclones. Williams et al. [3] obtained air-core size and shape in a 44-mm hydrocyclone and 150-mm LARCODEM. Cullivan and Williams [21] reported on the air-core shape obtained from EIT and ultrasound tomography and found them consistent with each other. Cullivan et al. [22] explained the air-core inception mechanism through CFD and attempted validation with the same EIT data. EIT and CFD results qualitatively were in good agreement for the flow structure in the hydrocyclone. Bond et al. [27] measured the air-core data at different feed pressures using ERT in a 50-mm hydrocyclone. Wood [28] determined the air-core data by a solid with tip in a 200-mm DSM cyclone body. Subramanian [29] mapped air-core profiles by GRT in a 350-mm DSM cyclone body and also measured density profiles along the radius at different axial positions. The air-core diameter was estimated by a high-speed camera in a Krebs 250-mm hydrocyclone and a 33-mm hydrocyclone [23, 30]. In most of the models applied to a cyclone, the interface that bounds the air-core is modeled as a fixed cylindrical surface, which greatly simplifies the problem. Due to the significant role of air-core in the hydrocyclone, many researchers have developed theoretical models to approximate the air-core radius [15, 31–33]. Recently, a semi-empirical model was proposed to predict the air-core diameter at different axial locations for a hydrocyclone operating with solids [34]. Despite the attention that the air-core modeling has received, most of the mathematical models above suffer from the lack of being validated against the measured air-core diameter of the hydrocyclone treating pulp and wide range of operating conditions.

Although air-core measurements were performed successfully by a number of researchers as compiled in Tab. 1, comprehensive data on air-core profiles with respect to hydrocyclone design parameters and operating conditions are very limited. Air-core profiles are not compared with respect to any alternative measurements. Only few researchers attempted to compare the air-core diameters by GRT and high-speed camera with theoretical CFD predictions [35, 36]. Nearly in all past research on ERT the air-core shape was assessed correctly, with low conductivity observed in the center of the hydrocyclone. In spite of the ERT advantage in terms of its much higher scanning rate, the key challenge is to obtain sufficiently accurate definitions of phase boundaries. The spatial resolution of ERT is relatively poor in comparison to other systems such as computed X-ray tomography and magnetic resonance imaging (MRI). The spatial resolution of the ERT is in the range of 5–10 % of the equipment diameter. Improvement in the image reconstruction algorithms would allow reconstructing accurately the conductivity distributions inside the two-phase flow systems.

Air-core profiles were measured by means of the fast-response ERT system and high-speed camera. The study involves mapping the conductivity distribution in a hydrocyclone operating mainly with water under spray discharge conditions. ERT data analysis is performed with diverse finite element method (FEM) meshes and different image reconstruction algorithms as part of forward and inverse methods, respectively. The air-core diameter is estimated by the measured conductivity distribution. The influence of design and operating conditions of the hydrocyclone on air-core size is studied in detail. Cross validation of air-core size by ERT measurements against the high-speed camera and CFD simulations is attempted.

3 Methodology

3.1 ERT Experiments

The high-speed ITS z8000 two-planar ERT system used in this work is designed based on a high-performance dual-plane ERT system with a data acquisition speed of 1000 dual frames per second. Plane 1 and plane 2 were situated at a distance of 0.32 m and 0.215 m from the bottom of the hydrocyclone. The ERT setup contained three parts, i.e., sensors, data acquisition system (DAS), and computer. The sensors were connected to the conical section of the hydrocyclone as illustrated in Fig. 1. The other end of the sensors was coupled to the DAS. The host computer and DAS were linked through the probe. Sixteen equally spaced electrodes (sensors) were fitted on the periphery of the hydrocyclone in each plane and there are two planes in the conical section. The rectangular-shape stainless-steel electrodes were connected to the DAS via cables. The distance between the two planes was 10 cm.

Before collecting the data by ERT, it was necessary to take a reference measurement since the system works on the principle of taking measurements and comparing these to known reference data. Initially, the hydrocyclone was filled with water by closing the spigot and the calibration was carried out. Afterwards, the hydrocyclone was run under various process conditions. The ERT system was employed to measure the voltage drop at all electrode pairs. An adjacent electrode strategy was used to obtain the voltage measurements. Electric current was applied between one pair of electrodes and the resultant voltage differences among the remaining 13 electrode pairs were determined by DAS. Experiments were conducted with water in a 76-mm diameter hydrocyclone fitted with the ERT system. The hydrocyclone dimensions are depicted in Fig. 2 a.

A scheme of the experimental setup is presented in Fig. 3. To determine the effect of changes in pressure, spigots, and vortex finder on the air-core diameter, 42 tests were conducted. Three levels of spigot, six levels of inlet pressure, and two levels of

Table 1. Summary of literature.

Entry	Authors	Important parameters	Remarks
1	Williams et al. [3]	Two planes, 16 electrodes, UMIST ERT, qualitative image reconstruction algorithm	Air-core imaging in 44-mm hydrocyclone, 150-mm LARCODEM. Qualitative air core measurement with shape and size
2	Bond et al. [27]	Eight planes, 16 electrodes, P1000ITS ERT, linear back projection algorithm	Estimation of air-core diameter by parametric reconstruction for different feed pressures of an operating 50-mm hydrocyclone
3	Williams et al. [25], Gutierrez et al. [26]	One plane, 16 electrodes, UMIST EIT, linear back projection algorithm	Particle distribution and fault underflow detection in a classifying and dewatering 44-mm cyclone
4	Wang et al. [37]	One plane, 16 electrodes, P2000 ERT and 50 ms per frame, modified sensitivity coefficient back projection (MSBP), multi-step inverse solution (STM)	Unsteady mixing dynamics of miscible liquids studied with different conductivities. STM provided more accurate data compared to MSBP algorithm.
5	Cullivan et al. [22]	EIT system, high-speed video imaging, ultrasound tomography, CFD	Cross-validated with CFD-predicted air-core size and behavior in a 50-mm hydrocyclone
6	Subramanian et al. [29]	Gamma ray tomography	Air-core profile measurement, mapping of densities along radial direction in a 350-mm DSM cyclone
7	Devullapalli et al. [30]	High-speed video imaging	Air-core diameter estimation in a 250-mm Krebs hydrocyclone
8	Ricard et al. [38]	ITS P2000 ERT, linear back projection algorithm	Application of ERT in multiphase processes important for pharmaceutical industries. Measurement of ERT concentration profiles for validation of CFD results in a mixing reactor
9	Gamio et al. [39]	ECT system, linear back projection algorithm	ECT for visualization of gas oil two-phase flows in pressurized loops

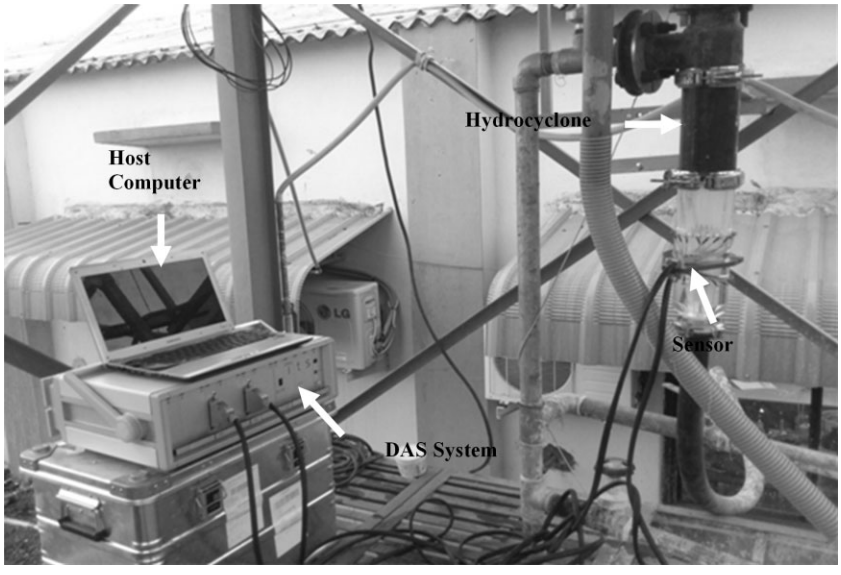

Figure 1. ERT setup with hydrocyclone rig.

vortex finder diameter variations were considered in the test matrix. The range of variables used in the experiments is given in Tab. 2. For a given feed pressure condition, the mass flow rate was calculated by collecting the overflow and underflow flow rates simultaneously for 10 s which was repeated for three times in order to get the average data.

3.2 High-Speed Video Imaging

An alternative method, the image processing technique was used to measure the air-core size for an operating cyclone. A digital camera, having 14.1 mega pixel resolutions with 10X optical zoom (a Sony-G lens) at 30 fps at 1280×720 pixels was adopted for air-core visualization. A total of minimum 10 seconds (nearly 300 frames) air-core recorded video is converted into a number of images. Nearly 30 images are averaged (per sec basis) to analyze air-core occupied diameters. The averaged air-core diameter and its associated standard deviations were reported. This data is used to cross validate the air-core data obtained from ERT and CFD.

3.3 CFD Modeling

To validate the ERT air-core data, the two-phase (water-air) CFD studies were also carried in the same 3-inch hydrocyclone. ANSYS's ICEM was employed for creating geometry, meshing, and applying appropriate boundary conditions. Grid independence is tested and a 3D body-fitted grid with 156 600 nodes is used for simulations. The mesh used for the simulation is displayed in Fig. 2 1 b. The CFD model uses volume-of-fluid (VOF) for re-

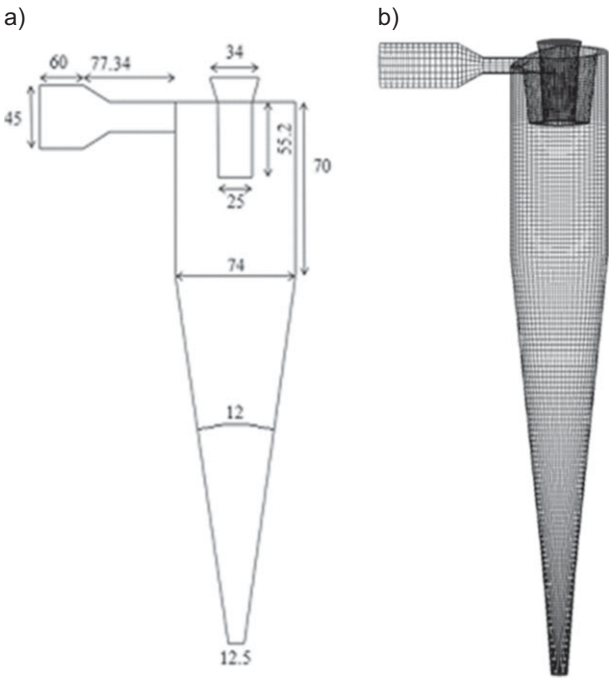

Figure 2. (a) Scheme of a 3-inch hydrocyclone; (b) mesh used for the simulations.

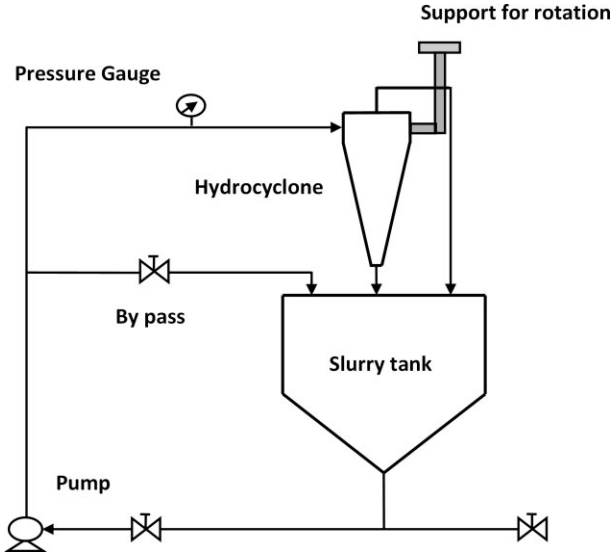

Figure 3. Hydrocyclone process flow diagram.

Table 2. Range of variable conditions used in the experimental study.

Variable	Variation range
Cyclone diameter	76 mm
Inlet diameter	45 mm
Vortex finder diameter	18, 25 mm
Spigot diameter	10, 12.5, 15, 20 mm
Pressure	5, 10, 15, 20, 25, 30 psi

solving the air-water interface and large eddy simulation (LES) for turbulence modeling. A number of simulations were performed with the commercial software FLUENT. The CFD strategy for simulating the air-core in the hydrocyclone is similar to Narasimha et al. [40]. Initially, simulations were set up to obtain convergence data for the water case. An air-core was then allowed to develop by setting the backflow air volume fraction to unity for the overflow and underflow boundary conditions. After the air-core was fully formed, the mean volume fraction of air was extracted from unsteady state statistics at plane 1 and plane 2.

4 Results and Discussion

4.1 ERT Data Analysis

Image reconstruction is one of the most important and difficult part of ERT data analysis. In this work, different FEM mesh sizes were used as part of the forward solution and the three reconstruction algorithms were adopted as part of inverse solution of ERT data. Raw data extracted from the ITS ERT tool site software served as input for reconstruction algorithms. The three identified reconstruction algorithms were Gauss-Newton (GN)-one step, Tikhonov regularization matrix (TRM), and total variation (TV). The GN-one step algorithm [41] is an improved method over the linear-back projection algorithm. In the TRM method [42], the calibrated voltage data is incorporated into the algorithm from which the solution is obtained for the measured air-core data. TV regularization is one technique to permit image regularization without imposing smoothing [43]. To avoid the smoothing for process imaging, the TV technique is recommended.

Data analysis is performed using the specific data set of a cyclone operating at 15 psi pressure, 20 mm diameter of spigot, and 25 mm diameter of vortex finder. The number of frames collected by means of the ERT system is nearly 3000, roughly at about 6–8 s of operation. Fig. 4 presents the obtained ERT system voltage measurements, reference voltage measurements, and relative changes between the reference and actual measurements. The horizontal axis denotes the pair of different electrode measurements from 1 to 13. This display is often used to know whether the system is operating with minimal noise or not. The working ERT system has two planes, so the graph is indicating the measurements for two planes. The average data of these frames is used to extract the raw voltage measurement. These average voltages are given as an input file for the MATLAB program which is built with various FEM meshes and reconstruction algorithms [44].

4.1.1 Mesh Quality Effect on Air-Core Resolution

Voltages generated from averaging the collected frames are employed to get the conductivity distribution for the different mesh types. Various mesh sizes from very coarse to fine quality are used for calculation of conductivity and voltages by the FEM technique as part of the forward solution. The conductivity tomograms obtained for different mesh sizes and GN-one

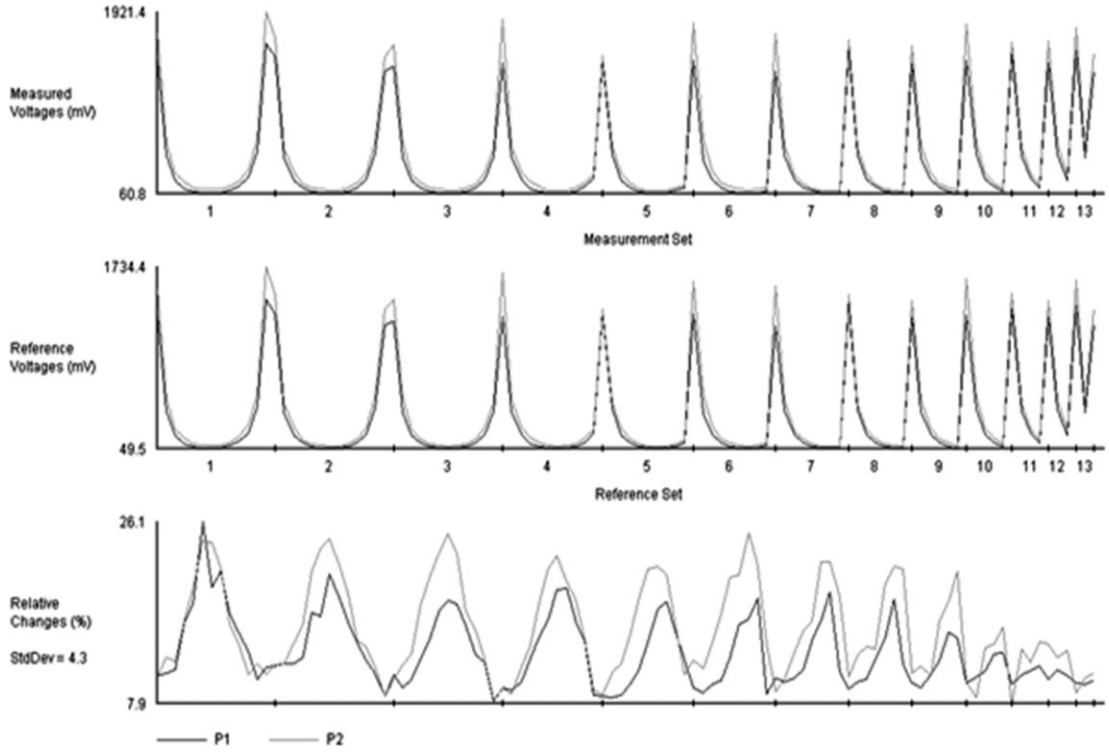

Figure 4. ERT voltage measurements at two planes in the conical section of the cyclone.

step algorithm are depicted in Fig. 5. From the reconstructed images one can observe that a coarse mesh of 256 elements exhibits a high numerical diffusive nature compared to other mesh sizes. For a mesh size of 2304 elements onwards, the tomograms indicate the minimal diffusive nature of conductivity. Therefore, the M2304 mesh (M indicates mesh and the number 2304 denotes the total number of elements used in that mesh) is identified as the optimal FEM mesh, which minimizes the numerical diffusion of conductivity distributions. The conductivity plots across the radial position of plane 2 in

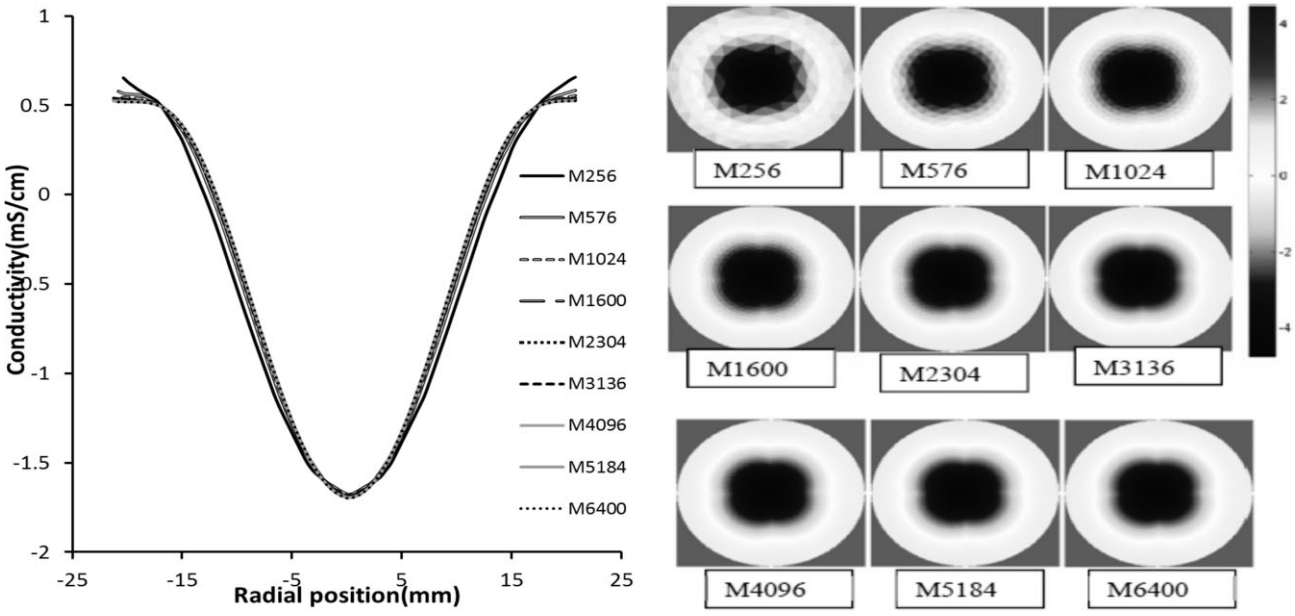

Figure 5. Conductivity profiles for different mesh sizes. (a) Averaged radial distribution; (b) reconstructed tomograms using GN-one step algorithm for a cyclone operating at 15 psi pressure, 20 mm spigot, and 25 mm vortex finder.

the hydrocyclone are plotted for various mesh sizes. It is found that the diffusive nature of conductivity is low for the fine mesh when compared to the coarse mesh. Consequently, by increasing the mesh size, the numerical diffusive nature of the conductivity decreases.

4.1.2 Effect of Image Reconstruction Algorithm

GN-one step, Tikhonov regularization, and TV image reconstruction algorithms are applied to get the conductivity tomograms from the surface voltages. The comparison of these algorithms is made with the specific data set of a cyclone operating at 15 psi pressure, 20 mm diameter of spigot, and 25 mm diameter of vortex finder by adopting the optimal mesh size (M2304). The conductivity tomograms are plotted in Fig. 6 a for these three different image reconstruction algorithms. The obtained tomographic image from the ITS tool, in which the modified sensitivity back projection (MSBP) algorithm is applied, is also displayed in Fig. 6 a. The conductivity distribution across the radial position of plane 2 is indicated in Fig. 6 b for these image reconstruction algorithms. The conductivity profiles are plotted along the center axis of the plane. It is observed that the TV and Tikhonov regularization algorithms are calculating the improved conductivity profiles in nature compared to the GN-one step algorithm.

The TV and Tikhonov algorithms based reconstruction data indicate a step change of conductivity distribution for the water-air system as expected in the hydrocyclone, whereas the GN-one step and MSBP are producing the very diffusive nature conductivity profiles. The high-speed digital camera measurements show a sharp boundary between the air-water phases which is clearly observed with the TV and Tikhonov algorithms. The ERT data analyzed using the mesh size of minimum >2000 elements and the TV or Tikhonov algorithms would be able to resolve the air-core interface correctly with water in a hydrocyclone. This ERT method analysis is adopted for all the cases of hydrocyclone ERT experiments. A parametric study of air-core profiles is attempted in the following work.

4.2 Estimation of Air-Core Size

Traditionally, the pixel-based image reconstruction from ERT measurements is a well-known problem. An alternative approach is required to get quantitative information from the ERT measurements. Such an approach is used here as parametric modeling. The conductivity profile within the fluid is modeled with a quadratic function requiring three parameters [24]. The air-core radius can be calculated using parametric modeling according to the following equation:

$$\sigma(r) = a + b\,(3\,r{-}2) + c\,(10\,r^2 - 12\,r + 3) \quad (1)$$

where σ is the conductivity, a, b, and c are parameters, and r is the position between the air-core and the boundary such that 0 corresponds to the air-core boundary and 1 to the wall of the hydrocyclone. Thus, the system was defined by four parameters including air-core radius and the other three are terms a, b, and c of the quadratic Eq. (1). The best fit to the measurements was calculated with the least squares metric technique. The primary reason for parametric modeling is the interpretation of the air-water interface position. The obtained air-core diameter from the parametric modeling and corresponding conductivity tomograms for the case of 12.5 mm spigot diameter and 25 mm vortex finder diameter are presented in Figs. 7 and 8.

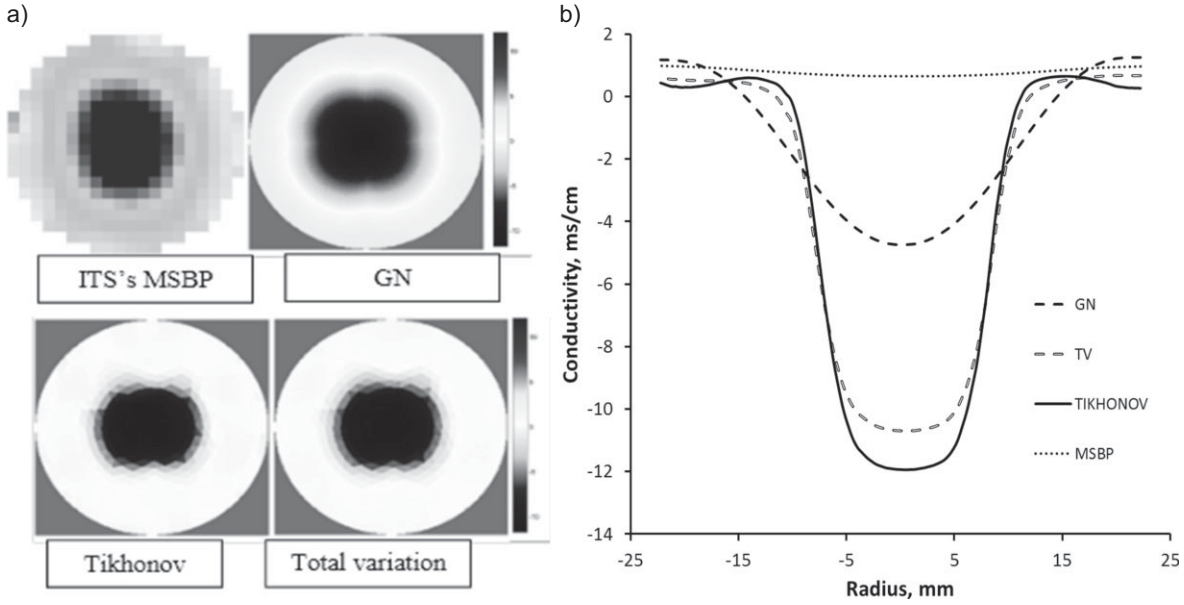

Figure 6. Conductivity profiles of (a) reconstructed tomograms, (b) averaged radial distribution using different algorithms for a cyclone operating at 15 psi pressure, 20 mm spigot, and 25 mm vortex finder.

The ERT conductivity tomograms reconstructed by three algorithms data for 12.5 mm spigot and 25 vortex finder of the cyclone operating at various pressures are displayed in Fig. 7. Compared to GN and TR algorithms, the TV algorithm-based conductivity data minimizes the numerical diffusive zone at all operating feed pressures. The same trend can be observed in Fig. 8 in terms of the estimated air-core diameters. GN-based ERT data overestimates the air-core sizes. Fig. 8 includes the measured air-core diameter from the high-speed digital camera at the same height. The change in air-core diameter with respect to the pressure is observed considering all measurement techniques.

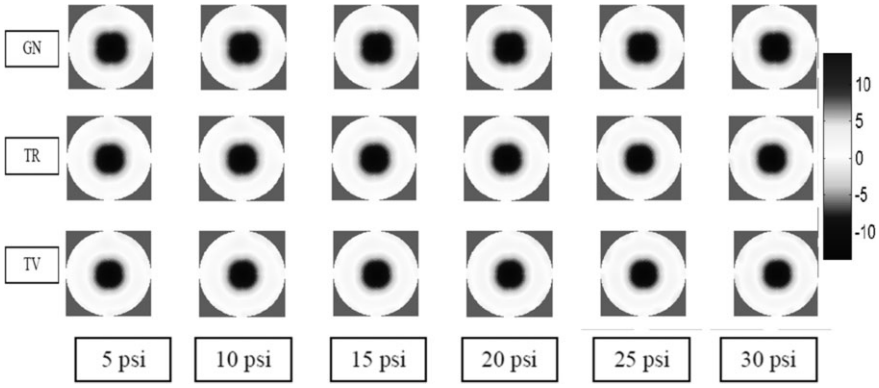

Figure 7. ERT conductivity tomograms for 12.5 mm spigot and 25 mm vortex finder of a 76-mm hydrocyclone.

4.3 Effect of Feed Pressure on Air-Core Size

In general, increasing the feed flow rate or inlet pressure causes a higher maximum tangential velocity (accounting for the increase of kinetic energy) in a given cyclone, which in turn leads to a decrease in the pressure at the hydrocyclone axis near the spigot. If the pressure is lowered near the spigot zone, the air can be easier sucked in through the bottom of the cyclone. Hence, the air-core diameter increases with inlet pressure as demonstrated by the ERT tomograms in Fig. 9.

The radial conductivity distribution for a 76-mm cyclone with 15 mm spigot diameter under different feed pressures is depicted in Fig. 10 a. This distribution was used to estimate the air-core diameter of the hydrocyclone by parametric modeling. The estimated air-core profiles are presented in Fig. 10 b for various spigots operating at different pressures.

The air-core diameter increases with higher pressure up to a certain limit which is in accordance to the theory. Increasing the pressure above this critical value leads to a decrease in the air-core diameter. This is also observed based on the data of the high-speed digital camera. The decline trend might be due to the air-phase compression or increased slip between the water-air interfaces.

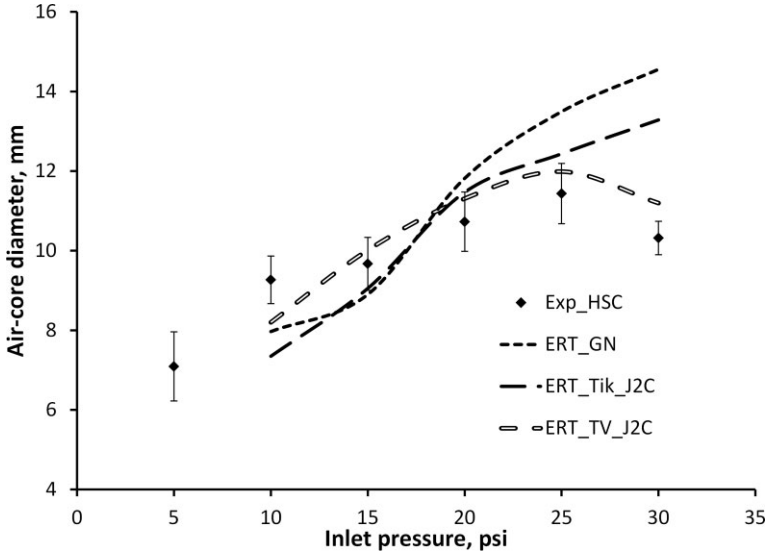

Figure 8. Comparison of air-core diameters by various algorithms against high-speed digital camera data for 12.5 mm spigot, 25 mm vortex finder, 76-mm hydrocyclone operating at different pressures.

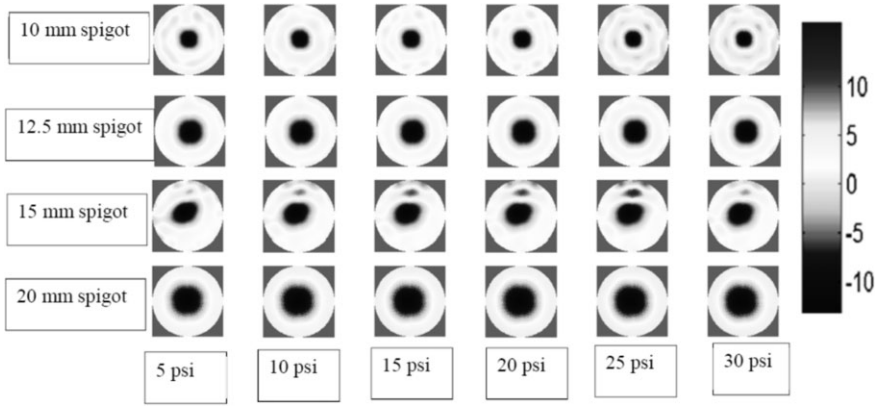

Figure 9. Comparison of ERT conductivity tomograms at different feed pressures and spigots for 25 mm vortex finder of a 76-mm hydrocyclone.

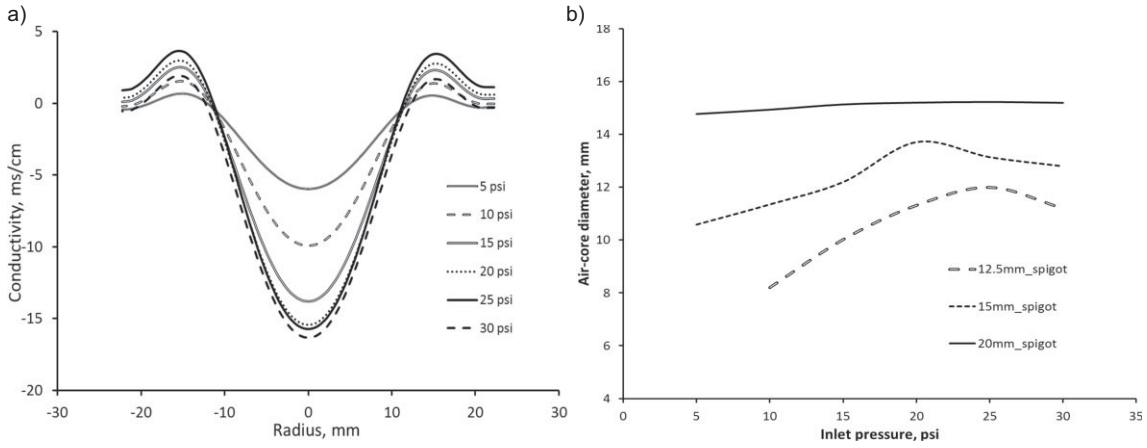

Figure 10. Conductivity profiles of (a) averaged radial distribution for 15 mm spigot, (b) estimated air-core profiles for different inlet pressures for a cyclone operating at 12.5, 15, and 20 mm spigots, respectively.

4.4 Effect of Spigot on Air-Core Size

As the spigot diameter increases, the low-pressure region of occupied area also becomes larger and a rise in the tangential velocity is observed. Because of the higher tangential velocity, the fluid flows towards the wall, resulting in more pressure drops in the central zone. Consequently, more air passes into the hydrocyclone from both orifices (underflow and overflow) which are exposed to the atmosphere.

The conductivity tomographic variation of the air-core diameter for different spigot diameters is also illustrated in Fig. 9. Fig. 10 b presents the estimated air-core profiles for various spigot diameters. With larger spigot diameter the air-core diameter increases in accordance to the theoretical trend. Variation of the air-core diameter with relation to the inlet pressure is not significantly differing with large spigot diameters, whereas it is very sensitive to feed pressure changes at smaller spigot diameters.

4.5 Validation of ERT Data

To validate the ERT air-core data, two-phase (water-air) CFD studies and high-speed digital camera measurements were carried out for the 3-inch hydrocyclone. The computations were performed for a spigot diameter of 10, 12.5, 15 mm at different feed velocities. The mass fluxes for each feed velocity condition were predicted using the reports option in FLUENT software. Mass flow rates at the inlet and two outlets were predicted and water spilt to underflow was calculated. The calculated water spilt to underflow was compared with experimental results. The water spilt to underflow for 12.5 mm spigot diameter of a 76-mm hydrocyclone is displayed in Fig. 11 a. It decreased with increasing feed velocity. The mean volume fraction of air along the axial position of the hydrocyclone is depicted as contour plot in Fig. 11 b.

The mean volume fraction of water at plane 2 of the ERT system and predicted CFD air volume contour at 21.5 mm from the

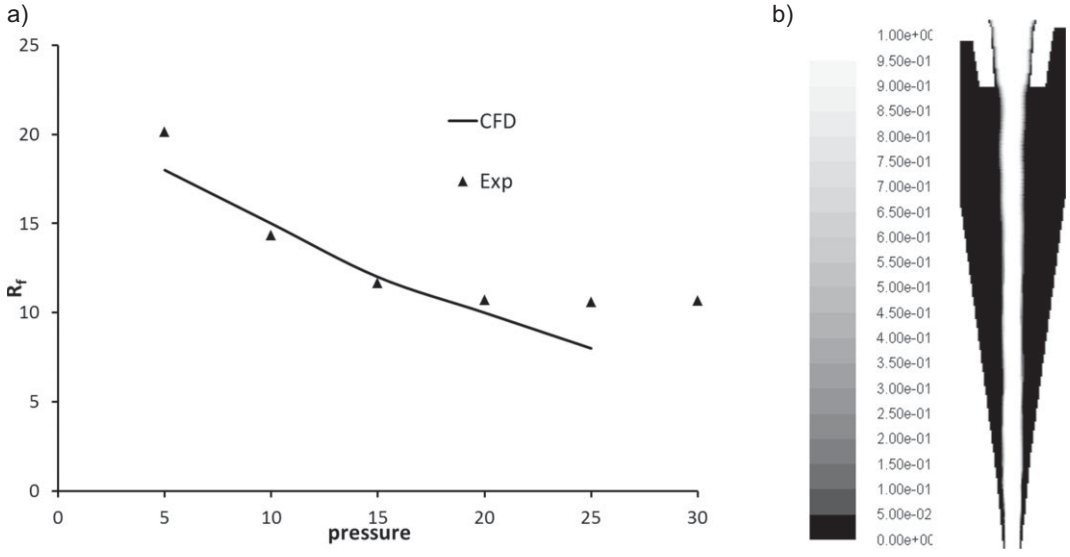

Figure 11. (a) Water spilt ratio obtained from experiments and CFD predictions; (b) simulated air-core profile.

bottom of the hydrocyclone are presented in Fig. 12. From these contours it follows that air-core formation occurred at the central part along the axial position of the hydrocyclone.

The air-core diameter obtained from parametric modeling for 12.5 and 15 mm spigot diameters and 25 mm vortex finder diameter of a given hydrocyclone is compared with the results from the high-speed camera in Fig. 13. These results are also compared with the CFD technique. The change in air-core diameter with respect to the pressure is obvious in all measurement techniques.

The CFD results are following the same trend as the findings obtained with the digital camera. The percentage of error of the air-core diameter was calculated for ERT data with the air-core diameter obtained from the digital camera experiments and also for CFD data related to the same high-speed camera data. The maximum error was 44 % for CFD data in case of estimating the air-core diameter at 30 psi feed pressure and for 15 mm spigot diameter and 25 mm vortex finder diameter of a 76-mm hydrocyclone. The minimum error was 0.388 % for 25 psi feed pressure for 10 mm spigot diameter and 25 mm vortex finder diameter of a 76-mm hydrocyclone. The average errors of the air-core diameter estimated between the CFD data and the digital camera data for 10, 12.5, and 15 mm spigot diameters were 8.2 %, 19.76 %, and 15.38 %, respectively. Tab. 3 compares the air-core diameters using ERT, HSV, and CFD.

In the same way the percentage of standard error in estimating the air-core diameter with ERT data was calculated with respect to the high-speed camera data. For different feed pressures with 12.5 mm and 15 mm spigot diameters of a 76-mm hydrocyclone the percentage error of the air-core diameter for ERT with respect to the HSC data was determined. The average percentage of standard error for 12.5, 15, and 20 mm spigot diameters calculated for ERT data against the digital camera data were 6.7 %, 13.53 %, and 9.72 %, respectively.

5 Multiphase Flow Measurements

Most of the scarce ERT literature on multiphase flow predictions is related to two-phase flow measurements but there are few works reporting on industrial multiphase flows. Ricard et al. [38] studied the effect of impeller speed, feed solids addition, and amount of settling product on the base of the mixing reactor to the formation of paracetamol using ERT. They also validated the CFD results with the experimentally calculated ERT values. Gamio [39] applied ECT to visualize gas oil two-phase flows in pressurized loops and observed different flow regimes through ECT images.

Similarly, ERT can be employed to measure the concentration profiles inside a hydrocyclone using the predicted conductivity values by Maxwell's equations [45]. These profiles can be further taken to validate CFD results. The authors made an attempt to extend this method for hydrocyclones operated with solids. ERT conductivity profiles were extracted at two different pressures for water only and 10 wt % slurry with a 15-mm spigot (Fig. 14 a). The multiphase air-core behavior was

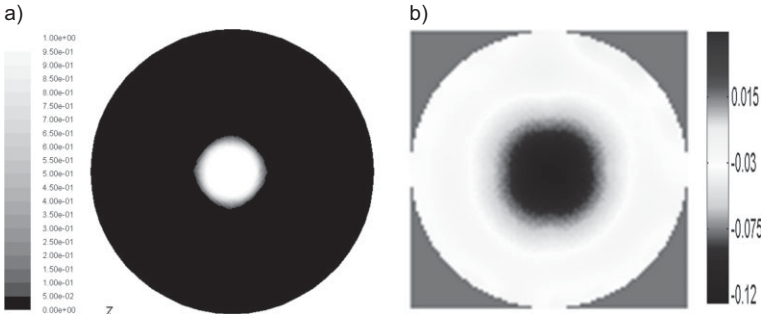

Figure 12. (a) Predicted mean volume fraction of water contour by CFD; (b) conductivity tomogram by ERT for 12.5 mm spigot of a 76-mm hydrocyclone at plane 2 of ERT (21.5 mm from bottom).

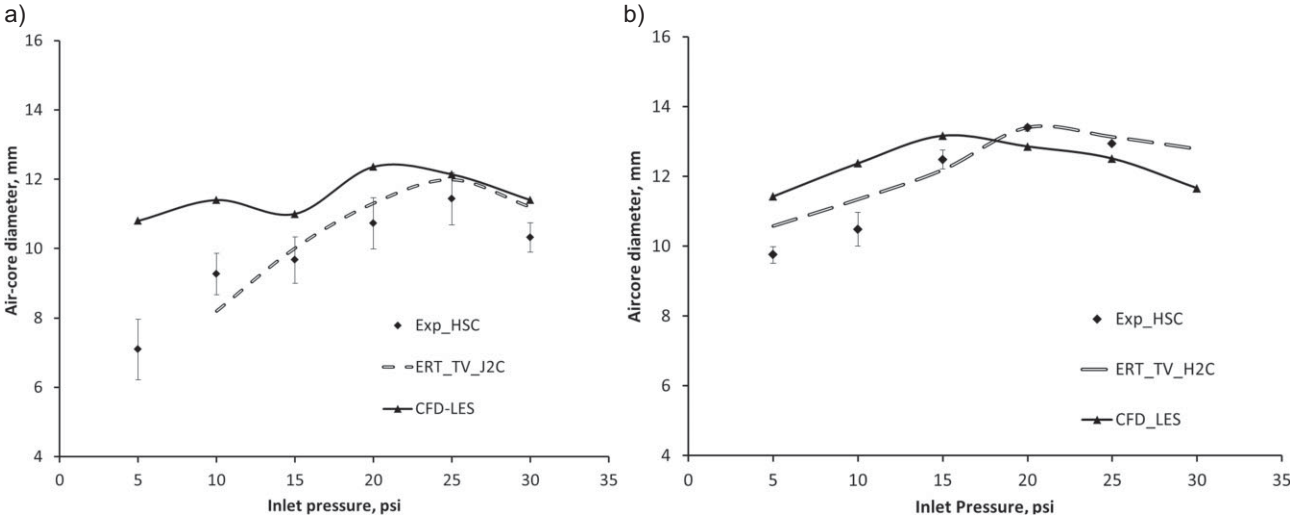

Figure 13. Comparison of air-core diameter determined by HSC algorithm, ERT-TV algorithm, and CFD technique for (a) 12.5 mm spigot, (b) 15 mm spigot of a 76-mm hydrocyclone.

Table 3. Cross validation of air-core diameters.

Spigot [mm]	Vortex finder [mm]	Pressure [psi]	Air core diameter [mm]		
			CFD predicted	HSV measured	ERT measured
12.5	25	5	10.763	7.093	–
		10	11.385	9.268	8.2
		15	10.942	9.669	10.014
		20	12.316	10.728	11.309
		25	12.123	11.435	11.988
		30	11.367	10.318	11.619
15	25	5	11.438	9.749	10.583
		10	12.371	10.483	11.335
		15	13.149	12.482	12.216
		20	12.838	13.387	13.408
		25	12.501	12.9331	13.123
		30	11.619	12.613	12.812

found to be similar to the two-phase air-core except the size. The air-core size was reduced with an increase in the feed solids concentration. Low conductivity values were observed near the air-core and wall sections, indicating a higher solid particle concentration. CFD predictions of air-core at different feed solids concentration along with the water only case are displayed qualitatively in Fig. 14 b. As the feed solids concentration increases, the amount of water present near the wall reduces and becomes higher around the air-core. This signifies that more solid particles are present at the wall section. Therefore, ERT measurements indicate low conductivity near the walls (Fig. 14 a, 10 wt % solids case).

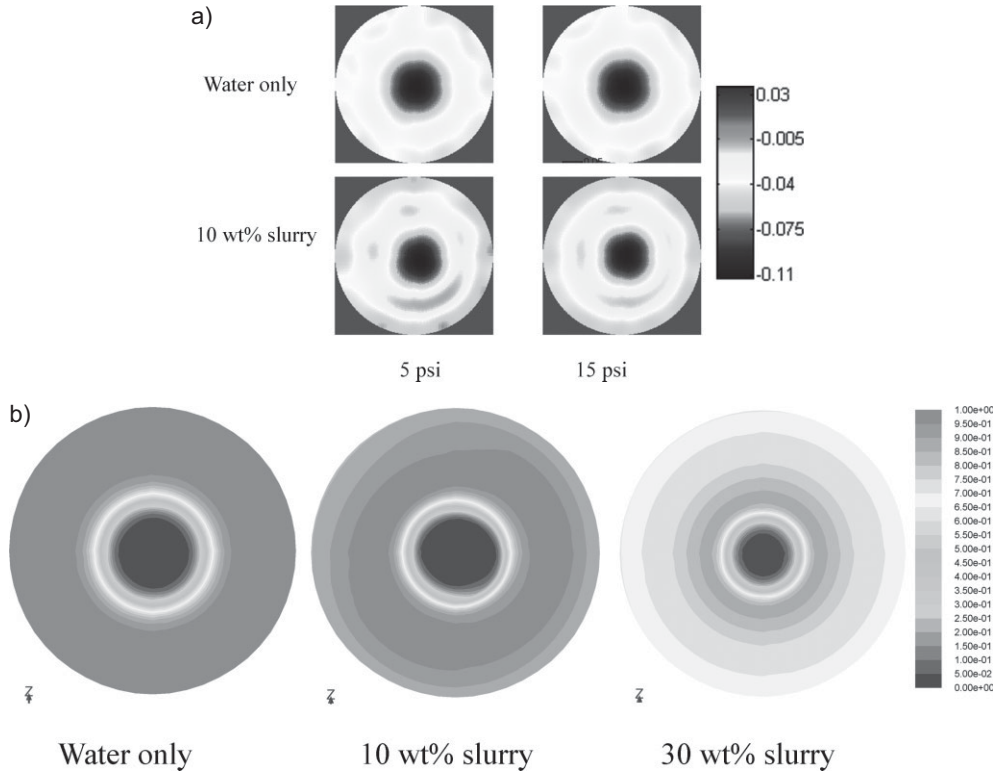

Figure 14. (a) Comparison of air-core diameter variation for only water and feed slurry at two feed pressures by ERT; (b) variation of air-core diameter at different feed solids concentrations using CFD.

6 Conclusions

The measurement of two-phase distributions was mapped by a dual-plane high-speed ERT system. Experiments were carried out in a 76-mm hydrocyclone and the results were presented in terms of the air-core diameter and its size variation for different feed flow rates and design variables. The tomographic images were created through the forward FEM solution and inverse reconstruction algorithms. GN-one step, Tikhonov regularization, and TV image reconstruction algorithms were applied to obtain conductivity tomograms from the raw surface voltages. Air-core profiles from the conductivity distributions were estimated by a parametric modeling approach. ERT confirmed that the air-core diameter increases with higher feed flow rate and larger spigot diameter of the operating cyclone. In order to compare the reliability of the ERT measurements, the same cyclone geometry was used for simulating the air-core by CFD. A VOF two-phase model coupled with an LES turbulence model enabled simulation of the air-core within the cyclone. A series of CFD simulations were run together with ERT measurements. Additional validation was performed with digital camera-based air-core diameters. The estimated ERT data were compared with CFD mean air-core profiles. The ERT data exhibit a maximum error of 20 % in comparison to CFD data and of 14 % with respect to the digital camera data. The air-core size measurement for a cyclone operating with 10 wt % slurry at two inlet pressures is assessed qualitatively against the CFD predictions.

The authors have declared no conflict of interest.

References

[1] F. Dickin, M. Wang, *Meas. Sci. Technol.* **1996**, *7*, 247–260.
[2] D. L. George, J. R. Torczynski, K. A. Shollenberger, T. J. O'Hern, S. L. Ceccio, *Int. J. Multiphase Flow* **2000**, *26*, 549–581.
[3] R. A. Williams, O. M. Ilyas, *Chem. Eng. J.* **1995**, *56*, 135–141.
[4] R. A. Williams, O. M. Ilyas, T. Dyakowski, *Coal Prep.* **1995**, *15*, 149–163.
[5] R. A. Williams, X. Jia, R. M. West, N. Climpson, J. A. Kostuci, D. Payton, *Miner. Eng.* **1999**, *12*, 1245–1252.
[6] H. Jin, M. Wang, R. A. Williams, *Chem. Eng. J.* **2007**, *130*, 179–185.
[7] D. C. Barber, A. D. Seagar, *Clin. Phys. Physiol. Meas. Suppl. A* **1987**, *8*, 47–54.
[8] C. J. Kotre, *PhD Thesis*, Newcastle University **1993**.
[9] T. J. Yorkey, J. G. Webster, W. J. Tompkins, *IEEE Trans. Biomed. Eng.* **1987**, *34*, 843–852.
[10] A. Wexler, B. Fry, M. R. Neuman, *Appl. Opt.* **1985**, *24*, 3985–3992.
[11] M. Z. Abdullah, W. F. Conway, T. Dyakowski, R. C. Waterfall, *Workshop on Tomographic Techniques for Process Design and Operation*, Manchester, England **1993**.
[12] M. Wang, A. Dorward, D. Vlaev, R. Mann, *Chem. Eng. J.* **2000**, *77*, 93–98.
[13] A. Barrientos, R. Sampio, F. Concha, *XVIII Int. Mineral Processing Congress*, Sydney, May **1993**.
[14] O. Castro, *MEngSci Thesis,* University of Queensland, Brisbane **1990**.
[15] F. Concha, A. Barrientos, J. Montero, R. Sampio, *Int. J. Miner. Process.* **1996**, *44–45*,743–749.
[16] T. Dyakowski, B. Williams, *Powder Technol.* **1996**, *87*, 43–47.
[17] A. J. Lynch, T. C. Rao, *XI Int. Mineral Processing Congress*, Cagliari, **1975**.
[18] K. Nageswararao, *PhD Thesis*, University of Queensland, Brisbane **1978**.
[19] M. Narasimha, *PhD Thesis*, University of Queensland, Brisbane **2010**.
[20] M. A. Bennet, R. A. Williams, *Miner. Eng.* **2004**, *17*, 605–614.
[21] J. C. Cullivan, R. A. Williams, C. R. Cross, *Trans. IChem* **2003**, *81A*, 455–465.
[22] J. C. Cullivan, R. A. Williams, T. Dyakowski, C. R. Cross, *Miner. Eng.* **2004**, *17*, 651–660.
[23] Q. Luo, J. R. Xu, *4th Int. Conf. on Hydrocyclones,* Southampton, England, September **1992**.
[24] R. M. West, X. Jia, R. A. Williams, *1st World Congress on Industrial Process Tomography*, Buxton, April **1999**.
[25] R. A. Williams, F. Dickin, J. A. Gutiérreza, T. Dyakowski, M. S. Beck, *Control Eng. Pract.* **1997**, *5 (2)*, 253–256.
[26] J. A. Gutiérreza, T. Dyakowski , M. S. Beck, R. A. Williams, *Powder Technol.* **2000**, *108*, 180–184.
[27] J. Bond, J. C. Cullivan, N. Climpson, T. Dyakowski, I. Faulks, X. Jia, J. A. Kostuch, D. Payton, M. Wang, S. J. Wang, R. M. West, R. A. Williams, *1st World Congress on Industrial Process Tomography*, Buxton, April **1999**.
[28] J. C. Wood, *PhD Thesis*, University of Queensland, Brisbane **1990**.
[29] V. J. Subramanian, *PhD Thesis*, University of Queensland, Brisbane **2002**.
[30] B. Devullapalli, *PhD Thesis*, University of Utah, Salt Lake City, UT **1997**.
[31] A. Barrientos, F. Concha, *SME Publ.* **1992**, 287–295.
[32] M. R. Davidson, *Int. Symp. on Numerical Methods for Multiphase Flows*, Lake Tahoe, NV, June **1994**.
[33] P. R. Steffens, W. J. Whiten, S. Appleby, J. Hitchins, *Int. J. Miner. Process.* **1993**, *39*, 61–74.
[34] M. Narasimha, A. N. Mainza, P. N. Holtham, *XXVI Int. Mineral Processing Congress*, New Delhi, September **2012**.
[35] M. Brennan, P. N. Holtham, M. Khanal, R. Morrison, *5th World Congress on Industrial Process Tomography*, Bergen, September **2007**.
[36] J. Delgadillo, R. K. Rajamani, *Int. J. Comput. Fluid Dyn.* **2009**, *23*, 189–197.
[37] M. Wang, W. Yin, *IChemE, Part A* **2001**, *79*, 883–886.
[38] F. Ricard, C. Brechtelsbauer, X. Y. Xu, C. J. Lawrence, *Chem. Eng. Res. Des.* **2005**, *83*, 794–805.
[39] J. C. Gamio, J. Castro, L. Rivera, J. Alamilla, F. Garcia-Nocetti, L. Aguilar, *Flow Meas. Instrum.* **2005**, *16*, 129–134.
[40] M. Narasimha, M. Brennan, P. N. Holtham, *Int. J. Miner. Process.* **2006**, *80*, 1–15.
[41] N. Polydorides, *PhD Thesis*, University of Manchester **2002**.
[42] T. Kriz, J. Dedkova, E. Gescheidtov, *Progress in Electromagnetics Research Symp. Proc.*, Moscow, August **2009**.
[43] L. I. Rudin, S. Osher, E. Fatemi, *Physica D* **1992**, *60*, 10.
[44] A. Adler, W. R. B. Lionheart, *Physiol. Meas.* **2006**, *27 (5)*, 25.
[45] J. C. Maxwell, *A Treatise on Electricity and Magnetism*, 2nd ed., Calendar Press, Oxford **1881**.

Research Article: The air-core is one of the most important flow characteristics in hydrocyclones. Air-core profiles were measured by a dual-plane fast-response electrical resistance tomography system and high-speed camera. The influence of design and operating conditions of the hydrocyclone on air-core size is studied. Three reconstruction algorithms were adopted. Results are validated against simulations and camera data.

Air-Core Size Measurement of Operating Hydrocyclone by Electrical Resistance Tomography

A. Rakesh, V. T. S. R Kumar Reddy, M. Narasimha*

Chem. Eng. Technol. **2014**, *37 (5)*, XXX ... XXX

DOI: 10.1002/ceat.201300672